D11

NASTRAN IMPLEMENTATION OF AN ISOPARAMETRIC DOUBLY-CURVED QUADRILATERAL SHELL ELEMENT

By

A. B. Potvin and R. D. Leick
Exxon Production Research Company; Houston, Texas

SUMMARY

A quadrilateral shell element, CQUAD4*, has been added to level 15.5 and subsequently to level 16.0 of NASTRAN. The element exhibits doubly-curved surfaces and uses bi-quadratic interpolation functions. Reduced integration techniques are used to improve the performance of the element in thin-shell problems. Several details of previous authors' (ref. 1) work are clarified with respect to the present NASTRAN implementation. The creation of several new bulk data items is discussed along with a special module, GPNORM, to process SHLNORM bulk data cards. In addition to the theoretical basis for the element stiffness matrix, consistent mass and load matrices are presented.

Several potential sources of degenerate behavior of the element are investigated. Guidelines for proper use of the element are suggested. Performance of the element on several widely-published classical examples is demonstrated. The results show a significant improvement over presently available NASTRAN shell elements for even the coarsest meshes. Potential applications to two classes of practical problems are discussed.

INTRODUCTION

Until recently, only the CQUAD2 and its analog CTRIA2 were available in NASTRAN for analyzing shells of arbitrary geometry. Compared to current shell element technology, these elements are subject to the following limitations:

- o Faceted (flat) surface geometry is poorly adapted to model curved shapes.

* After the initial implementation of the new element was completed, the authors became aware of a similar proprietary element under development by the MacNeal-Schwendler Corporation which used the name CQUAD4. The reader should take care not to confuse these two identically named elements, since it is our understanding that the formulation and performance are quite different.

- Lower order polynomials used in membrane formulation cause element to be excessively stiff for in-plane deformation.

- While the enforced linear variation of the normal slope along the sides of the element guarantees interelement compatibility, it causes the bending behavior of the element to be quite stiff as well.

- In problems exhibiting thick shell and/or three-dimensional behavior over certain regions, the CQUAD2 element is an inadequate model and is difficult to interface with three dimensional elements.

To alleviate these problems development work on the present (CQUAD4) element was begun with the intention of implementing it in NASTRAN Level 15.5. The efforts were partially successful but full implementation was not achieved until NASTRAN Level 16.0 became available last year. The choice of the element was primarily influenced by the need to accurately represent curved surfaces as well as thick shell/3-D behavior. Such extremely accurate elements as Cowper's (ref. 2) and Dupuis' (ref. 3) were rejected due to the present authors' preference to adhere to the standard six degrees of freedom (dof) preferred by the majority of the user community. Although the theoretical development has often been presented elsewhere (refs. 1, 4, 5, 6, 7, and 8), we choose to repeat enough of the development to clarify certain issues which caused difficulty in the present implementation.

SYMBOLS (Scalars)

Values are given in both SI and U.S. Customary Units. The measurements and calculations were made in U.S. Customary Units.

a, b	Plate edge dimensions
D	Shell flexural rigidity $[Et^3/12(1-\nu^2)]$
E	Elastic modulus
g_{1i}, g_{2i}, g_{3i}, h_{3i}	Components of interpolation derivative arrays
k	Shear correction factor
L	Structure length dimension
$N_i(\xi, \eta, \zeta)$	Interpolation function for node i
p	Constant pressure load on element
P	Concentrated load magnitude
q	Displacement value
R	Mean (midsurface) radius
t_i	Thickness at node i
u, v, w	Translational displacements at a point in basic coordinate system
u', v', w'	Translational displacements at a point in local coordinate system
u_i, v_i, w_i	Translational displacements at node i
v_{1x}^i, v_{1y}^i, v_{1z}^i	Components of unit vector defining local x axis at node i
v_{2x}^i, v_{2y}^i, v_{2z}^i	Components of unit vector defining local y axis at node i
V_{3x}^i, V_{3y}^i, V_{3z}^i	Components of the shell normal at node i

x, y, z	Basic cartesian coordinate variables
x', y', z'	Local cartesian coordinate variables
x_i, y_i, z_i	Basic cartesian coordinates at node i
α_i, β_i	Rotational displacements at node i
$\gamma_{x'y'}, \gamma_{x'z'}, \gamma_{y'z'}$	Shearing strain components in local coordinate system
$\varepsilon_{x'x'}, \varepsilon_{y'y'}, \varepsilon_{z'z'}$	Direct strain components in local coordinate system
ν	Poisson's ratio
ω	Natural frequency of structure
ξ, η, ζ	Curvilinear coordinate variables
ξ_i, η_i, ζ_i	Curvilinear coordinate at node i
$\sigma_{x'x'}, \sigma_{y'y'}, \sigma_{z'z'}$	Direct stress components in local coordinate system
$\tau_{x'y'}, \tau_{x'z'}, \tau_{y'z'}$	Shearing stress components in local coordinate system
ϕ_{ij}	Component of transformation matrix
ρ	Mass density per unit volume

SYMBOLS (Matrices and Vectors)

[ALPHAT]	Diagonal matrix of nodal thicknesses times local x rotation
[BETAT]	Diagonal matrix of nodal thicknesses times local y rotation
[B']	Strain-displacement relation referenced to local coordinates
$[B_i']$	Strain-displacement relation pertaining to node i
[DELTAT]	Array of translational displacements at nodes
[D']	Constitutive relation in local coordinate system
$\vec{F}$	Consistent load vector for element
$[G_i]$	Derivative array transformed to local coordinates
$[H_i]$	Derivative array transformed to local coordinates pertaining to $\partial/\partial\zeta$ operator
[J]	Jacobian matrix relating (x, y, z) and (ξ, η, ζ) systems
[K]	Element stiffness matrix referenced to basic coordinates
[M]	Element mass matrix referenced to basic coordinates
$\vec{n}$	Third row of Jacobian - Interpolated value of nodal normals
$\vec{N}$	Vector of nodal interpolation functions
$[\bar{N}]$	Array of nodal interpolation functions
$\vec{s}$	First row of Jacobian - vector tangent to surface ζ = const
$\vec{t}$	Second row of Jacobian - vector tangent to surface ζ = const
$\vec{v}_s$	Unit vector tangent to surface ζ = const, defining local x' axis
$\vec{v}_t$	Unit vector tangent to surface ζ = const, defining local y' axis
$\vec{v}_n$	Unit vector normal to surface ζ = const, defining local z' axis
$\vec{v}_{1i}$, $\vec{v}_{2i}$, $\vec{v}_{3i}$	Unit vectors defining local tangent coordinates at node i

$\vec{V}_1, \vec{V}_2, \vec{V}_3$	Vectors defining the coordinate system for nodal rotations
[V1TAN]	Array of local x direction vectors at nodes
[V2TAN]	Array of local y direction vectors at nodes
[V3NORM]	Array of shell normals at nodes
[XCOORD]	Array of nodal coordinates
$\vec{\delta}_i$	Displacement dof at node i
$\vec{\delta}$	Collection of nodal displacement vectors
$\vec{\varepsilon}'$	Strain components in local coordinates
$[\theta]$	Local/global transformation matrix (direction cosines)
$\vec{\sigma}'$	Stress components in local coordinates
$[\phi]$	Transformation from (x', y', z') system to (ξ, η, ζ) system
$[\Omega]$	Differential operator matrix for computing strains

THE STIFFNESS MATRIX

Basic Assumptions

Figure 1 shows the geometry of a typical element. The curvilinear coordinate system (ξ, η, ζ) is used where ξ and η lie in the middle surface of the element while ζ is directed through the thickness. Each of these coordinates is allowed to vary from -1 to +1 on opposite faces of the element. We adopt the customary assumption of shell theory that the strain component ($\varepsilon_{z'z'}$) in the thickness direction is neglected compared to the other strains. The input items describing the element geometry include the basic coordinates at each of the eight mid-surface nodes (GRID cards) plus the vectors normal to that surface at each node (SHLNORM cards). The length of each normal vector is taken to be the thickness at that node. The thickness is interpolated quadratically over the element. At present only homogeneous, isotropic, materials (MAT1 cards) are allowed. The element is not available for heat transfer problems nor are thermal load vectors calculated.

Interpolation Functions

The nodal coordinates are related to the basic coordinates by the equation:

$$\begin{Bmatrix} x \\ y \\ z \end{Bmatrix} = [\text{XCOORD}] \cdot \vec{N} + \frac{\zeta}{2} \cdot [\text{V3NORM}] \cdot \vec{N} \qquad (1)$$

where

$$[\text{XCOORD}] = \begin{bmatrix} x_1 & x_2 & \cdots & x_8 \\ y_1 & y_2 & \cdots & y_8 \\ z_1 & z_2 & \cdots & z_8 \end{bmatrix}$$

$$[\text{V3NORM}] = \begin{bmatrix} v_{3x}^1 & v_{3x}^2 & \cdots & v_{3x}^8 \\ v_{3y}^1 & v_{3y}^2 & \cdots & v_{3y}^8 \\ v_{3z}^1 & v_{3z}^2 & \cdots & v_{3z}^8 \end{bmatrix}$$

$$\vec{N} = \langle N_1 \quad N_2 \quad \cdots \quad N_8 \rangle^T$$

Details of the biquadratic interpolation functions (Ni) and their derivatives are given in Appendix A.

The translational displacements are chosen as u, v, and w in the x, y, and z directions respectively. Two rotations, α_i and β_i, are defined about the local axes, $\vec{v}_{1i}$ and $\vec{v}_{2i}$, tangent to the mid-surface at each node (i). The choice of these two local axes is discussed in Appendix B.

We may relate the nodal displacements to the continuous displacement representation in a manner analagous to equation (1).

$$\begin{Bmatrix} u \\ v \\ w \end{Bmatrix} = [DELTAT] \cdot \vec{N} + \frac{\zeta}{2} \cdot [V1TAN] \cdot [ALPHAT] \cdot \vec{N} - \frac{\zeta}{2} \cdot [V2TAN] \cdot [BETAT] \cdot \vec{N} \quad (2)$$

where

$$[DELTAT] = \begin{bmatrix} u_1 & u_2 & \cdots & u_8 \\ v_1 & v_2 & \cdots & v_8 \\ w_1 & w_2 & \cdots & w_8 \end{bmatrix}$$

$$[V1TAN] = \begin{bmatrix} v^1_{1x} & v^2_{1x} & \cdots & v^8_{1x} \\ v^1_{1y} & v^2_{1y} & \cdots & v^8_{1y} \\ v^1_{1z} & v^2_{1z} & \cdots & v^8_{1z} \end{bmatrix}$$

$$[V2TAN] = \begin{bmatrix} v^1_{2x} & v^2_{2x} & \cdots & v^8_{2x} \\ v^1_{2y} & v^2_{2y} & \cdots & v^8_{2y} \\ v^1_{2z} & v^2_{2z} & \cdots & v^8_{2z} \end{bmatrix}$$

$$[ALPHAT] = \begin{bmatrix} \alpha_1 t_1 & 0 & \cdots & 0 \\ 0 & \alpha_2 t_2 & \cdots & 0 \\ \vdots & \vdots & & \vdots \\ 0 & 0 & \cdots & \alpha_8 t_8 \end{bmatrix}$$

$$[BETAT] = \begin{bmatrix} \beta_1 t_1 & 0 & \cdots & 0 \\ 0 & \beta_2 t_2 & \cdots & 0 \\ \vdots & \vdots & & \vdots \\ 0 & 0 & \cdots & \beta_8 t_8 \end{bmatrix}$$

Coordinate Transformations

The relation between the curvilinear coordinates (ξ, η, ζ) and the basic coordinates (x, y, z) is commonly called the Jacobian, [J], defined as:

$$[J] = \begin{bmatrix} \partial x/\partial\xi & \partial y/\partial\xi & \partial z/\partial\xi \\ \partial x/\partial\eta & \partial y/\partial\eta & \partial z/\partial\eta \\ \partial x/\partial\zeta & \partial y/\partial\zeta & \partial z/\partial\zeta \end{bmatrix} = \begin{Bmatrix} \vec{s}^T \\ \vec{t}^T \\ \vec{n}^T \end{Bmatrix} \qquad (3)$$

Using equation (1) we can write out these expressions as:

$$\vec{s} = \begin{Bmatrix} \partial x/\partial\xi \\ \partial y/\partial\xi \\ \partial z/\partial\xi \end{Bmatrix} = [XCOORD] \cdot \partial\vec{N}/\partial\xi + \frac{\zeta}{2} \cdot [V3NORM] \cdot \partial\vec{N}/\partial\xi \qquad (4)$$

$$\vec{t} = \begin{Bmatrix} \partial x/\partial\eta \\ \partial y/\partial\eta \\ \partial z/\partial\eta \end{Bmatrix} = [XCOORD] \cdot \partial\vec{N}/\partial\eta + \frac{\zeta}{2} \cdot [V3NORM] \cdot \partial\vec{N}/\partial\eta \qquad (5)$$

$$\vec{n} = \begin{Bmatrix} \partial x/\partial\zeta \\ \partial y/\partial\zeta \\ \partial z/\partial\zeta \end{Bmatrix} = \frac{1}{2} \cdot [V3NORM] \cdot \vec{N} \qquad (6)$$

where $\partial\vec{N}/\partial\xi = < \partial N_1/\partial\xi \quad \partial N_2/\partial\xi \quad \ldots \quad \partial N_8/\partial\xi >^T$

$\partial\vec{N}/\partial\eta = < \partial N_1/\partial\eta \quad \partial N_2/\partial\eta \quad \ldots \quad \partial N_8/\partial\eta >^T$

The explicit forms of $\partial Ni/\partial\xi$ and $\partial Ni/\partial\eta$ are given in Appendix A. Physically the $\vec{s}$ and $\vec{t}$ vectors may be considered tangent to the surface ζ = constant, while the $\vec{n}$ vector is merely the interpolated value of the node normals and may not be exactly normal to that surface at the position (ξ, η, ζ).

Perhaps the most confusing point of the cited references is the use of still another local coordinate system for definition of the stresses and strains. The need for this additional (x', y', z') system arises from the definition of the basic shell assumptions (particularly the neglect of the through-the-thickness direct strain, $\varepsilon_{z'z'}$). We wish to define, at any point in the element, a local (z') axis which is normal to the surface ζ = constant along with two other orthogonal axes (x', y') which are tangent to that surface. Since we have previously determined that $\vec{s}$ and $\vec{t}$ are tangents to the surface, we can determine a normal vector as:

$$\vec{V}_n = \vec{s} \times \vec{t} \tag{7}$$

and

$$\vec{v}_n = \vec{V}_n / |\vec{V}_n| \tag{8}$$

The other two unit vectors defining the local axes ($\vec{v}_s$ and $\vec{v}_t$) are computed in a manner analagous to that given in Appendix B. Thus, x' is measured along the $\vec{v}_s$ vector, y' is measured along the $\vec{v}_t$ vector, and z' is measured along the $\vec{v}_n$ vector. We can define the transformation [θ] as:

$$[\theta] = [\vec{v}_s \quad \vec{v}_t \quad \vec{v}_n] \tag{9}$$

So

$$\begin{Bmatrix} x \\ y \\ z \end{Bmatrix} = [\theta] \begin{Bmatrix} x' \\ y' \\ z' \end{Bmatrix} \tag{10}$$

and

$$\begin{Bmatrix} u \\ v \\ w \end{Bmatrix} = [\theta] \begin{Bmatrix} u' \\ v' \\ w' \end{Bmatrix} \tag{11}$$

The Strain-Displacement Relation

Using the newly developed local system and noting that $\varepsilon_{z'z'}$ is neglected, we write the basic definition:

$$\vec{\varepsilon}' = \begin{Bmatrix} \varepsilon_{x'x'} \\ \varepsilon_{y'y'} \\ \gamma_{x'y'} \\ \gamma_{x'z'} \\ \gamma_{y'z'} \end{Bmatrix} = \begin{bmatrix} \partial/\partial x' & 0 & 0 \\ 0 & \partial/\partial y' & 0 \\ \partial/\partial y' & \partial/\partial x' & 0 \\ \partial/\partial z' & 0 & \partial/\partial x' \\ 0 & \partial/\partial z' & \partial/\partial y' \end{bmatrix} \begin{Bmatrix} u' \\ v' \\ w' \end{Bmatrix} \tag{12}$$

We make use of equations (10) and (3) to develop the relation

$$\begin{Bmatrix} \partial/\partial x' \\ \partial/\partial y' \\ \partial/\partial z' \end{Bmatrix} = [\theta]^{-1} \begin{Bmatrix} \partial/\partial x \\ \partial/\partial y \\ \partial/\partial z \end{Bmatrix} = [\theta]^{-1} [J]^{-1} \begin{Bmatrix} \partial/\partial \xi \\ \partial/\partial \eta \\ \partial/\partial \zeta \end{Bmatrix} \qquad (13)$$

Define

$$[\phi] = [\theta]^{T} [J]^{-1} \qquad (14)$$

Where $[\theta]^{-1}$ is equal to $[\theta]^{T}$, since $[\theta]$ is defined to be an orthonormal matrix. Then $[\phi]$ will have the form:

$$\begin{bmatrix} \phi_{11} & \phi_{12} & 0 \\ \phi_{21} & \phi_{22} & 0 \\ \phi_{31} & \phi_{32} & \phi_{33} \end{bmatrix} \qquad (15)$$

A complete derivation of the terms in $[\phi]$ is given in Appendix C. However, $[J]^{-1}$ is best evaluated numerically at each integration point and cannot be written out explicitly. We combine equations (13), (14), and (15) with (12) to arrive at:

$$\vec{\varepsilon}' = \begin{bmatrix} \phi_{11}\,\partial/\partial\xi + \phi_{12}\,\partial/\partial\eta & 0 & 0 \\ 0 & \phi_{21}\,\partial/\partial\xi + \phi_{22}\,\partial/\partial\eta & 0 \\ \phi_{21}\,\partial/\partial\xi + \phi_{22}\,\partial/\partial\eta & \phi_{11}\,\partial/\partial\xi + \phi_{12}\,\partial/\partial\eta & 0 \\ \phi_{31}\,\partial/\partial\xi + \phi_{32}\,\partial/\partial\eta + \phi_{33}\,\partial/\partial\zeta & 0 & \phi_{11}\,\partial/\partial\xi + \phi_{12}\,\partial/\partial\eta \\ 0 & \phi_{31}\,\partial/\partial\xi + \phi_{32}\,\partial/\partial\eta + \phi_{33}\,\partial/\partial\zeta & \phi_{21}\,\partial/\partial\xi + \phi_{22}\,\partial/\partial\eta \end{bmatrix} \begin{Bmatrix} u' \\ v' \\ w' \end{Bmatrix}$$

$$= [\Omega] \begin{Bmatrix} u' \\ v' \\ w' \end{Bmatrix} \qquad (16)$$

Finally we use (11) along with (2) to substitute the appropriate expression for the displacements $< u' \quad v' \quad w' >$

$$\vec{\varepsilon}' = [\Omega]\,[\theta]^{T}[DELTAT] \cdot \vec{N} + [\Omega] \cdot [\theta]^{T} \cdot [V1TAN] \cdot [ALPHAT] \cdot \vec{N} \cdot \frac{\zeta}{2}$$

$$- [\Omega] \cdot [\theta]^{T} \cdot [V2TAN] \cdot [BETAT] \cdot \vec{N} \cdot \frac{\zeta}{2} \qquad (17)$$

By carrying out the indicated operations to allow the differential operator [Ω] to appropriately interact with ζ and $\vec{N}$ and by rearranging terms, we arrive at the relation:

$$\vec{\varepsilon}' = [B'] \vec{\delta} \tag{18}$$

where $\vec{\delta} = < \vec{\delta}_1 \quad \vec{\delta}_2 \quad . \; . \; . \quad \vec{\delta}_8 >^T$

and $\vec{\delta}_i = < u_i \quad v_i \quad w_i \quad \alpha_i \quad \beta_i >^T$

The explicit form of [B'] is shown in Appendix D.

The Stress-Strain Relation

Again referring to the primed local coordinates, the constitutive law is:

$$\vec{\sigma}' = [D'] \vec{\varepsilon}' \tag{19}$$

where $\vec{\sigma}' = < \sigma_{x'x'} \quad \sigma_{y'y'} \quad \tau_{x'y'} \quad \tau_{x'z'} \quad \tau_{y'z'} >^T$

and (for a homogeneous isotropic material):

$$[D'] = \frac{E}{1-\nu^2} \begin{bmatrix} 1 & \nu & 0 & 0 & 0 \\ \nu & 1 & 0 & 0 & 0 \\ 0 & 0 & \frac{1-\nu}{2} & 0 & 0 \\ 0 & 0 & 0 & \frac{1-\nu}{2k} & 0 \\ 0 & 0 & 0 & 0 & \frac{1-\nu}{2k} \end{bmatrix} \tag{20}$$

Here k is used to improve the shear representation. The displacement assumption causes the shear to be constant through the thickness, whereas the proper distribution is closer to parabolic. The ratio of the strain energies of the two distributions (parabolic/constant) is 1.2 which is substituted for k.

The Element Stiffness Matrix (Subroutine KQUAD4)

The standard virtual work arguments lead to the stiffness computation as follows:

$$[K] = \int_{Vol} [B']^T [D'] [B'] \; dVol \tag{21}$$

The usual volumetric measure is dx dy dz. Here the variables of integration are ξ, η, and ζ. The conversion of the cartesian volume to the curvilinear volume is via the Jacobian. Thus,

$$dVol = dx\ dy\ dz = \det [J]\ d\xi\ d\eta\ d\zeta \tag{22}$$

$$\text{So} \qquad [K] = \int_{-1}^{1}\int_{-1}^{1}\int_{-1}^{1} [B']^T [D'] [B'] \det [J]\ d\xi\ d\eta\ d\zeta \tag{23}$$

The integration is carried out numerically using two Gauss points in each direction. While capable of properly integrating the element's volume, this "reduced" integration is not sufficient to exactly evaluate the complex polynomials produced by equation (23). This implies that, while ultimate convergence is assured, the behavior will not be either bounded or monotonic. However, several authors (ref. 4 and 9) have shown that, by purposely underestimating the energy, the performance of the element is enhanced. By taking [J] and [0] to be invariant through the thickness, it is possible to explicitly carry out the integration in ζ. We choose not to do so, however, in order to ensure complete generality of the formulation for both thin and thick shell cases.

Stress Recovery (Subroutines SQUD41 and SQUD42)

Once the elements are assembled and the system equations solved for the displacements, the user needs to know the element stresses as well. Combining equations (18) and (19) with $\vec{\delta}$ now known, we obtain:

$$\vec{\sigma}' = [D'] [B'] \vec{\delta} \tag{24}$$

Recall however that, in general, [B'] is a function of the curvilinear coordinates (ξ, η, ζ). $\vec{\sigma}'$ is therefore also a function of these coordinates, so we must choose which points we will use for stress evaluation. It is known that the numerical integration points are the best "samples" of the overall element stress field. Unfortunately the values of $\zeta = \pm 0.57735$ do not give the maximum stresses through the thickness if bending is present. We have compromised to select the eight points given by $\xi = \pm 0.57735$; $\eta = \pm 0.57735$, and $\zeta = \pm 1.0$ to allow evaluation of the stresses at the top and bottom surfaces of the element (c.f. diagram in Appendix A). Since the values of $\sigma_{x'x'}$, $\sigma_{y'y'}$ and $\tau_{x'y'}$* are evaluated in the (x', y', z') local system, the stress directions may not be meaningful to the user. Consequently, the principal stresses (σ_1, σ_2, and τ_{max}) are also calculated and form the additional portion of each line of output.

THE CONSISTENT MASS MATRIX (Subroutine MCQUD4)

For simplicity we will neglect the rotational inertias associated with the α and β degrees of freedom. This assumption is particularly

*Notice that $\tau_{x'z'}$ and $\tau_{y'z'}$ are zero on the top and bottom surfaces.

appropriate for thin and moderately thick shells. It allows us to reference everything to the mid-surface ($\zeta = 0$). In particular:

$$[M] = \int_{Vol} \rho\, [\bar{N}]^T\, [\bar{N}]\, dVol \tag{25}$$

Choosing ρ = constant and making use of the above assumption (i.e. $\int_{-1}^{1} d\zeta \equiv t$)

$$[M] = \rho \int_{A} t\, [\bar{N}]^T\, [\bar{N}]\, dA \tag{26}$$

where
$$[\bar{N}] = \left[\begin{array}{ccc:ccc:c:ccc} N_1 & 0 & 0 & N_2 & 0 & 0 & & N_8 & 0 & 0 \\ 0 & N_1 & 0 & 0 & N_2 & 0 & \cdots & 0 & N_8 & 0 \\ 0 & 0 & N_1 & 0 & 0 & N_2 & & 0 & 0 & N_8 \end{array}\right]$$

In general ρ may be allowed to vary quadratically over the element in a manner similar to the thickness. This feature is not required for most cases of interest.

Since $\zeta = 0$ on the midsurface, we must resort to the device of computing the unit area in curvilinear coordinates as (using equations (4) and (5)):

$$dA = dx\, dy = |\vec{s} \times \vec{t}|\, d\xi\, d\eta \tag{26}$$

where $|\vec{s} \times \vec{t}|$ may be interpreted as the projection on the normal vector $\vec{v}_n$ of the normal vector associated with infinitesimal area, $dx \cdot dy$. Thus,

$$[M] = \rho \int_{-1}^{1} \int_{-1}^{1} t\, [\bar{N}]^T\, [\bar{N}]\, |\vec{v}_n|\, d\xi\, d\eta \tag{27}$$

In this case the full three-point Gauss integration must be used to properly evaluate the expression.

THE CONSISTENT LOAD VECTOR (Subroutines PLOAD4 and PWORK)

We derive the expression for a constant pressure (p) normal to the mid-surface of the element. As before, a quadratic variation of the pressure would cause no inherent difficulties. The development is entirely analagous to that used for the consistent mass matrix. Thus,

$$\vec{F} = p \int_{-1}^{1} \int_{-1}^{1} [\bar{N}]^T \vec{v}_n \, d\xi \, d\eta \qquad (28)$$

Again, the three-point Gauss rule is used to evaluate the expression.

SPECIAL NASTRAN CONSIDERATIONS

New Bulk Data Cards

Three new Bulk Data cards have been added to NASTRAN in conjunction with the new element. They are:

CQUAD4 - describing the element connectivity
PLOAD4 - specifying the elements to which constant pressure (p) is applied at the mid-surface
SHLNORM - inputting the direction vector of the normal to the shell surface at each grid point.

A complete description of each of these items is found in Appendix E.

Module to Process Shell Normals*

A new module, GPNORM, has been coded which converts the "external" grid point ID's on a SHLNORM card to the appropriate internal SIL's. The module also transforms the normal vector into the basic coordinate system for the problem and writes the results on the output data block SHLNRM. The DMAP calling sequence for the module is:

```
GPNORM    GEOM1,EQEXIN,BGPDT,CSTM / SHLNRM $
```

GPNORM must be added to the DMAP rigid format immediately prior to the TA1 module. SHLNRM must be added as the final input data block of TA1.

Augmented ECPT and EST Data Blocks*

The make up of the EST (and by analogy the ECPT) for the CQUAD4 element follows the standard format for the first 43 words.

Word	Contents
1	Element ID
2	Material ID
3-10	8 Grid Point SIL's
11-42	8 sets of Grid Point CSID's plus basic x, y, z coordinates
43	Element Temperature

*The idea to use GPNORM to process the shell normals as well as the technique for augmenting the ECPT and EST data blocks is credited to Miles Hurwitz of NSRDC.

The formulation of the element requires the components of the shell normals. These must be appended to the EST by subroutine TA1A.

44-67	8 sets of x, y, z components of the shell normals in basic coordinates

Subroutine TA1B performs a similar augmenting process for the ECPT data block.

VERIFICATION

Consider the limiting case of a square, simply supported flat plate* subjected to two load conditions, 1) a central load normal to the plate and 2) a uniform normal pressure. Figure 2 indicates that excellent convergence to the Timoshenko (ref. 10) result can be obtained with a 1 x 1 or at most a 2 x 2 grid. Note, however, that the usual bound theorems are not available with this particular element due to the use of reduced integration.

The next step in analytical complexity is represented by the problem portrayed in Figure 3, a pinched cylinder with free ends.* According to Timoshenko, the radial deflection at the point of application of the load, for the geometry given, should be -2.76 mm (-0.1087 in.). Timoshenko's result is based on an assumption of inextensional deformation which neglects the middle surface strain of the shell. The CQUAD4 element gives a slightly higher result of -2.89 mm (-0.1139 in.) for a 325 degree of freedom model of one-eighth of the cylinder. Cantin and Clough (ref. 11) predict a deflection of -2.87 mm (-0.1128 in.) using a cylindrical shell element model with 1200 degrees of freedom for one-eighth of the cylinder. Therefore, the CQUAD4 element, although not monotonic in convergence, does give excellent results for a minimum number of degrees of freedom.

An example problem which has become a classic for checking the response of shell-type elements is shown in Figure 4. The example is a cylindrical shell roof loaded by its own weight.* The ends of the shell are supported by diaphragms and the sides are free. It should be noted that two "exact" solutions have been quoted by various researchers. These two solutions may be attributed to Scordelis and Lo (ref. 12) and Cowper, Lindberg, and Olson (ref. 2).

Scordelis and Lo based their calculations on the theory of Gibson (ref. 13) essentially using shallow shell equations. Cowper, Lindberg, and Olson claimed that the shallow shell approximations were not used consistently when particular loadings were considered. They expanded the trigonometric representation of the load variation up to second order within each element by means of a Taylor Series. In addition

*When proper symmetry conditions are applied, only 1/4 or 1/8 of the entire structure need be modeled in each of these cases.

Cowper, et al. performed the integration of both the stiffness and load matrices over the area of the actual shell surface. Hence, the primary difference between the two "exact" solutions is the manner in which the consistent load matrices are formulated. The formulation of the present element follows more closely the method of Scordelis and Lo and hence will be compared to their "exact" solution.

Table 1 gives the computed displacements based on the grids defined in Figure 4. Note that excellent convergence is obtained. Figure 5 compares the predictions of the CQUAD4 element with the CQUAD2 element as well as slightly different formulations of the CQUAD4 element in the MARC (ref. 14) and SUPERB (ref. 15) finite element programs. Based on the results indicated in Figure 5 the CQUAD4 element is judged to be the most accurate.

To demonstrate the applicability of the CQUAD4 element in modeling dynamics problems, consider the rectangular cantilever plate vibration problem reported by Zienkiewicz (ref. 16) (see Figure 6). Compared in Figure 6 are test results by Plunkett (ref. 16) and finite element predictions based on a non-conforming triangle by Zienkiewicz and results from the CQUAD4 element. Note that even the two element idealization with the CQUAD4 element gives excellent results for the first four modes.

POTENTIAL SOURCES OF ELEMENT DEGENERACY

Three potential sources of element degeneracy were investigated. The first, non-rectangularity of the mesh, is illustrated in Figure 7. One quarter of a simply supported flat plate subjected to uniform pressure was modeled as shown with angular "offsets" or variations in the mesh rectangularity of up to 30°. As indicated in Figure 7 by the displacement prediction for the center of the plate, variations of up to 20° resulted in only 2% variation in deflection compared to the regular rectangular grid. The 30° variation resulted in a 7% difference. It would appear from these results that, for most applications, non-rectangularity will not have a significant effect on the results. However, care should be taken to maintain small angle variations of less than 30° as good practice.

The second potential source of degeneracy investigated was the shell thinness ratio, t/R. A pinched cylinder example was once again selected and the t/R ratio varied from 0.1 to 0.0001 as shown in Figure 8. By examining the product of the radial deflection at the point of load application and the flexural rigidity of the shell it is evident that no numerical instability exists even for very thin shells. Notice that for thicker shells (e.g. $t/R \geq 0.1$) Timoshenko's assumption of thin shell behavior is increasingly violated and some deviation of the finite element results from the classical solution is obtained.

The third potential source of element degeneracy to be investigated was similar to the mesh non-rectangularity of the flat plate problem. This example considers the event of a misalignment of the edges of the element with the directions of principal curvature in a shell idealization. Such a discretization may necessarily occur as a result of complex intersections of several shell elements. The pinched cylinder problem discussed previously was chosen as a simple limiting case. A 2 x 2 grid was selected for one-eighth of the cylinder and symmetry conditions were enforced. The element edges in the circumferential direction were allowed to vary from the direction of curvature as shown in Figure 9. The authors found that the radial deflection at the point of load application was virtually unaffected for the cases examined.

It may be concluded that, based upon the previously described investigations regarding element degeneracy which could possibly result from potential misuse, the CQUAD4 element appears to be exceptionally stable. Care should be used, however, in maintaining "relatively" rectangular element configurations.

APPLICATIONS

At least two potential sources of application for the CQUAD4 element exist in the offshore industry. Offshore drilling and production platforms are typically either a space frame of tubular members, commonly called a steel jacket structure, or a reinforced, prestressed concrete structure, commonly called a gravity structure. The welded intersections of tubular members in a steel jacket are called tubular joints and represent sources of potential fatigue problems due to high stress concentrations. The CQUAD4 element represents a significant increase in computational accuracy compared to the CQUAD2 element for conducting stress analyses of these tubular intersections.

The reasons for the improved accuracy are two-fold. The curved surface of the CQUAD4 element is its most obvious advantage. It was often necessary to use excessive CQUAD2 elements in otherwise coarse mesh regions of the joint model just to approximate the cylindrical geometry. An extremely important but less obvious advantage of the CQUAD4 element is its higher-order representation of the displacements, strains, and stresses, without having to expend any additional degrees of freedom. This advantage manifests itself in the degree of mesh refinement required to achieve a given level of accuracy. Whereas a FINE or EXTRA FINE mesh was required to achieve acceptable results using CQUAD2 elements (c.f. reference 17), a COARSE or MEDIUM mesh of CQUAD4 elements is sufficient. Such a typical mesh is shown in Figures 10 and 11 for a T-Joint and a K-Joint respectively. The mesh was automatically generated using the TKJOINT program described in reference (17). That program has recently been recoded to allow generation of the appropriate SHLNORM bulk data cards at each substructure grid point.

It should be pointed out that the CQUAD4 element does not specifically address the problem at the intersection line of the tubular members. Here the question is not whether the local behavior is more closely approximated by thin-shell or thick-shell theory, but how best to provide a transition to the three-dimensional state of stress which exists and how to include the weld geometry. Again the CQUAD4 element has an advantage over the CQUAD2 since it has been derived from a 20-node hexahedron. If a mesh of these 20-node elements is designed for the locality of the intersection, the transitional behavior between the CQUAD4 and the CIHEX2 should be smooth due to the compatibility of the basic interpolation functions. Unfortunately the transition between the two element types will still require a rather complex set of MPC's to be generated and this problem has not been adequately addressed at the time of publication.

The second source of potential application regards the structural modeling of the relatively thick shell cylinders and panels which comprise the base and towers of gravity structures (see Figure 12). Section A-A in Figure 12 illustrates the shell connections where the present element could be used. The individual cells are on the order of 20 meters in diameter and from 0.5 meters to 1.0 meters thick. The CQUAD2 element would be incapable of accurately modeling the structural behavior associated with this geometry. The CQUAD4 element provides the possibility of coupling with the CIHEX2 element to perform global stress analyses of these structures.

APPENDIX A

The biquadratic interpolation functions are well-known throughout the literature. They are repeated here along with their derivative forms only for the sake of completeness.

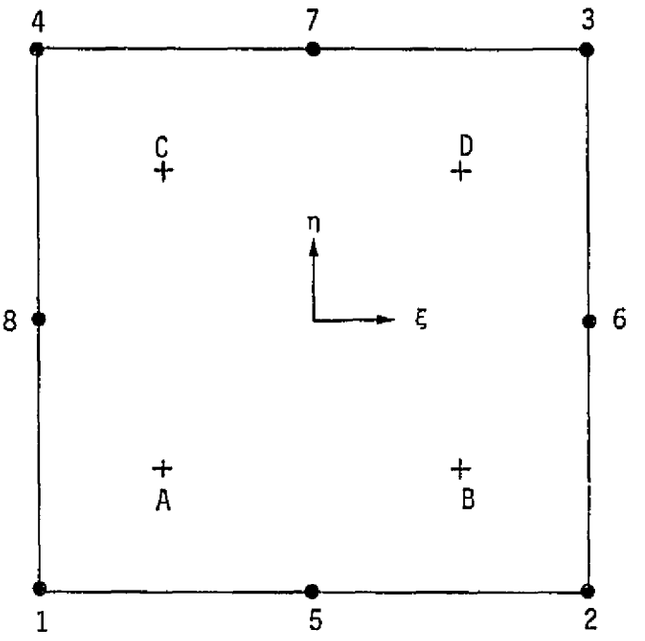

Node	ξ	η	ζ
1	-1	-1	0
2	1	-1	0
3	1	1	0
4	-1	1	0
5	0	-1	0
6	1	0	0
7	0	1	0
8	-1	0	0

Integration Point	ξ	η	ζ
A	-0.57735	-0.57735	±0.57735
B	0.57735	-0.57735	±0.57735
C	-0.57735	0.57735	±0.57735
D	0.57735	0.57735	±0.57735

Corner Nodes ($i = 1, 2, 3, 4$)

$$N_i = \frac{1}{4}(1 + \xi\xi_i)(1 + \eta\eta_i)(\xi\xi_i + \eta\eta_i - 1) \quad \text{(A-1)}$$

$$\partial N_i/\partial\xi = \frac{1}{4}\xi_i(1 + \eta\eta_i)(2\xi\xi_i + \eta\eta_i) \quad \text{(A-2)}$$

$$\partial N_i/\partial\eta = \frac{1}{4}\eta_i(1 + \xi\xi_i)(\xi\xi_i + 2\eta\eta_i) \quad \text{(A-3)}$$

Midside Nodes with $\xi_i = 0$ ($i = 5, 7$)

$$N_i = \frac{1}{2}(1 - \xi^2)(1 + \eta\eta_i) \quad \text{(A-4)}$$

$$\partial N_i/\partial\xi = -\xi(1 + \eta\eta_i) \quad \text{(A-5)}$$

$$\partial N_i/\partial\eta = \frac{1}{2}\eta_i(1 - \xi^2) \quad \text{(A-6)}$$

Midside Nodes with $\eta_i = 0$ ($i = 6, 8$)

$$N_i = \frac{1}{2}(1 + \xi\xi_i)(1 - \eta^2) \quad \text{(A-7)}$$

$$\partial N_i/\partial\xi = \frac{1}{2}\xi_i(1 - \eta^2) \quad \text{(A-8)}$$

$$\partial N_i/\partial\eta = -\eta(1 + \xi\xi_i) \quad \text{(A-9)}$$

APPENDIX B

At each node we are given the vector $\vec{V}_{3i}$ which is normal to the midsurface at that point. With reference to the basic (x, y, z) coordinate system, let $\hat{i}$ = (1 0 0) and $\hat{j}$ = (0 1 0). Choose $\vec{V}_{1i} = \hat{i} \times \vec{V}_{3i}$ which makes $\vec{V}_{1i}$ perpendicular to $\vec{V}_{3i}$ and the x axis. If $\vec{V}_{3i}$ is parallel to $\hat{i}$, then choose $\vec{V}_{1i} = \hat{j} \times \vec{V}_{3i}$ to remove the ambiguity. The third vector of the triad is then $\vec{V}_{2i} = \vec{V}_{3i} \times \vec{V}_{1i}$.

To compute the coordinate system transformation matrix, we normalize the components of each vector by its scalar length and form the set $[\vec{v}_{1i} \quad \vec{v}_{2i} \quad \vec{v}_{3i}]$ where

$$\vec{v}_{1i} = \vec{V}_{1i}/|\vec{V}_{1i}| \quad \text{etc.}$$

APPENDIX C

Equations (3-6) define the components of the Jacobian as:

$$[J] = \begin{Bmatrix} \vec{s}^T \\ \vec{t}^T \\ \vec{n}^T \end{Bmatrix} \tag{C-1}$$

The schematic form of the inverse may be written as:

$$[J]^{-1} = \frac{1}{\det [J]} [(\vec{t} \times \vec{n}) (\vec{n} \times \vec{s}) (\vec{s} \times \vec{t})] \tag{C-2}$$

Equations (7-9) define the local transform [θ] as

$$[\theta] = [\vec{v}_s \ \vec{v}_t \ \vec{v}_n] \tag{C-3}$$

where $\vec{v}_n$ was computed as the normal to the surface ζ = const by taking $\vec{s} \times \vec{t}/|\vec{s} \times \vec{t}|$ and $\vec{v}_s$ as well as $\vec{v}_t$ were defined to be perpendicular to $\vec{v}_n$. It is therefore clear that $\vec{v}_s$ and $\vec{v}_t$ will lie in the same plane as $\vec{s}$ and $\vec{t}$ but that $\vec{v}_n$ may not in general be considered parallel to $\vec{n}$.

Consider the computation of $[\phi] = [\theta]^T [J^{-1}]$

$$[\phi] = \frac{1}{\det [J]} \begin{Bmatrix} \vec{v}_s^T \\ \vec{v}_t^T \\ \vec{v}_n^T \end{Bmatrix} [(\vec{t} \times \vec{n}) (\vec{n} \times \vec{s}) (\vec{s} \times \vec{t})] \tag{C-4}$$

$$= \frac{1}{\det [J]} \begin{bmatrix} \vec{v}_s^T \cdot (\vec{t} \times \vec{n}) & \vec{v}_s^T \cdot (\vec{n} \times \vec{s}) & \vec{v}_s^T \cdot (\vec{s} \times \vec{t}) \\ \vec{v}_t^T \cdot (\vec{t} \times \vec{n}) & \vec{v}_t^T \cdot (\vec{n} \times \vec{s}) & \vec{v}_t^T \cdot (\vec{s} \times \vec{t}) \\ \vec{v}_n^T \cdot (\vec{t} \times \vec{n}) & \vec{v}_n^T \cdot (\vec{n} \times \vec{s}) & \vec{v}_n^T \cdot (\vec{s} \times \vec{t}) \end{bmatrix} \tag{C-5}$$

Now we know that $(\vec{s} \times \vec{t}) = \vec{v}_n = |\vec{v}_n| \cdot \vec{v}_n$. Therefore, since the dot product of perpendicular vectors is zero, we have $\vec{v}_s^T \cdot (\vec{s} \times \vec{t}) \equiv 0$. This completes the derivation of $[\phi]$. Notice that the terms ϕ_{31} and ϕ_{32} are not set to zero as was done in reference (4). The only time that these terms would be zero is when the vector $\vec{n}$ is exactly normal to the surface at the point (ξ, η, ζ). This event will only occur in the case of flat plates. The consequence of neglecting these two terms is to introduce an imbalance in the moment equilibrium of the shell (c.f. ref. 18).

APPENDIX D

We choose to divide the [B'] matrix into the following nodal partitions:

$$\vec{\varepsilon}' = [B_1' \quad B_2' \quad \ldots \quad B_8'] \begin{Bmatrix} \vec{\delta}_1 \\ \vec{\delta}_2 \\ \cdot \\ \cdot \\ \vec{\delta}_8 \end{Bmatrix} \tag{D-1}$$

We shall write out the expression for a typical partition $[B_i']$ by rearranging appropriate terms from equation (17):

$$[B_i'] = \left[[\Omega]\, N_i\, [\theta]^T + [\Omega]\, N_i\, \zeta\, \frac{t_i}{2}\, [\theta]^T \vec{v}_1{}^i \quad - [\Omega]\, N_i\, \zeta\, \frac{t_i}{2}\, [\theta]^T \vec{v}_2{}^i \right] \begin{Bmatrix} u_i \\ v_i \\ w_i \\ \alpha_i \\ \beta_i \end{Bmatrix} \tag{D-2}$$

Define

$$\begin{aligned} g_{1i} &= \phi_{11}\, \partial N_i/\partial\xi + \phi_{12}\, \partial N_i/\partial\eta \\ g_{2i} &= \phi_{21}\, \partial N_i/\partial\xi + \phi_{22}\, \partial N_i/\partial\eta \\ g_{3i} &= \phi_{31}\, \partial N_i/\partial\xi + \phi_{32}\, \partial N_i/\partial\eta \\ h_{3i} &= \phi_{33}\, N_i \end{aligned} \tag{D-3}$$

So

$$[G_i] = [\Omega]\, N_i = \begin{bmatrix} g_{1i} & 0 & 0 \\ 0 & g_{2i} & 0 \\ g_{2i} & g_{1i} & 0 \\ g_{3i} & 0 & g_{1i} \\ 0 & g_{3i} & g_{2i} \end{bmatrix} \tag{D-4}$$

and $[H_i] = \begin{bmatrix} 0 & 0 & 0 \\ 0 & 0 & 0 \\ 0 & 0 & 0 \\ h_{3i} & 0 & 0 \\ 0 & h_{3i} & 0 \end{bmatrix}$ (D-5)

Finally,

$$[B_i'] = [G_i]\,[\theta]^T + \frac{t_i}{2}\,(\zeta\,[G_i] + [H_i])\,[\theta]^T\,\vec{v}_1{}^i - \frac{t_i}{2}\,(\zeta\,[G_i] + [H_i])\,[\theta]^T\,\vec{v}_2{}^i$$

APPENDIX E

BULK DATA DECK

Input Data Card CQUAD4 Quadrilateral Element Connection

Description: Defines a homogeneous quadrilateral membrane and bending element (QUAD4) of the structural model.

Format and Example:

1	2	3	4	5	6	7	8	9	10
CQUAD4	EID	MID	G1	G2	G3	G4	G5	G6	abc
CQUAD4	72	13	13	14	15	16	21	22	ABC
+bc	G7	G8	TH						
+BC	23	24	29.2						

Field	Contents
EID	Element identification number (Integer > 0)
MID	Identification number of a MAT1 material card (Default is EID) (Integer > 0)
G1,G2,G3,G4 G5,G6,G7,G8	Grid point identification numbers of connection points (Integer > 0; G1 ≠ G2 ≠ G3 ≠ G4 ≠ G5 ≠ G6 ≠ G7 ≠ G8)
TH	Material property orientation angle in degrees (Real) The sketch below gives the sign convention for TH.

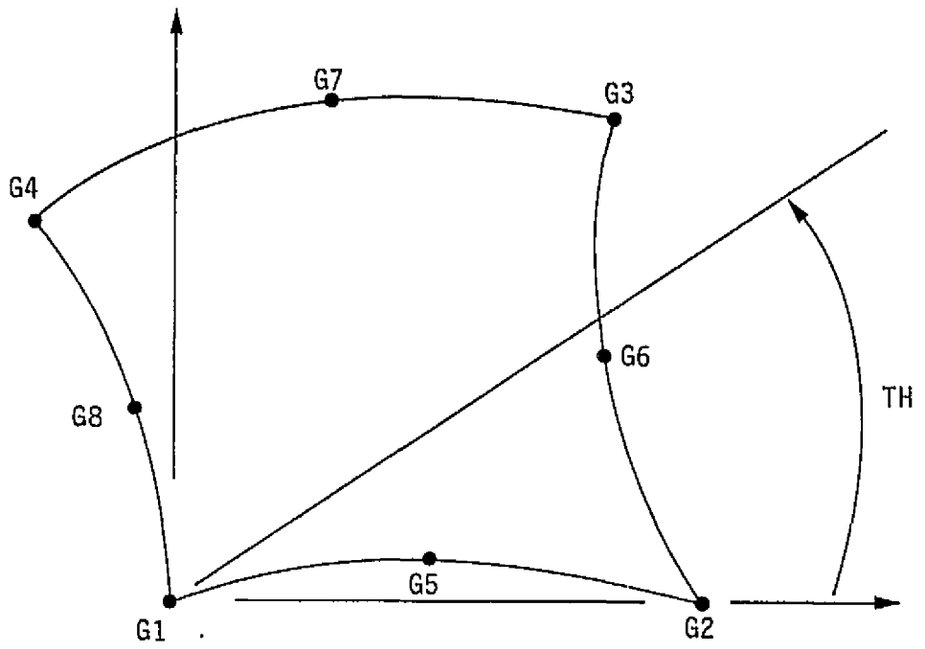

Remarks:

1. Element identification numbers must be unique with respect to all other element identification numbers.

2. Grid points G1 through G4 are corner nodes and must be ordered consecutively around the perimeter of the element in a counter clockwise direction. G5 through G8 are midside nodes and must have similar ordering where:

   G5 lies between G1 and G2
   G6 lies between G2 and G3
   G7 lies between G3 and G4
   G8 lies between G4 and G1

3. The continuation card must be present.

Input Data Card PLØAD4 Pressure Load

Description: Defines a uniform static pressure load applied to two-dimensional elements. Only QUAD4 elements may have a pressure load applied to them via this card.

Format and Example:

1	2	3	4	5	6	7	8	9	10
PLØAD4	SID	P	EID	EID	EID	EID	EID	EID	
PLØAD4	21	-3.6		4	16		2		

Alternate Form

PLØAD4	SID	P	EID1	"THRU"	EID2				
PLØAD4	1	30.4	16	THRU	48				

Field	Contents
SID	Load set identification number (Integer > 0)
P	Pressure value (Real), positive pressure value indicates pressure in the negative normal direction.
EID EID1 EID2	Element identification number (Integer > 0; EID1 < EID2)

Remarks:

1. EID must be 0 or blank for omitted entrys.
2. Load sets must be selected in the Case Control Deck (LØAD=SID) to be used by NASTRAN.
3. At least one positive EID must be present on each PLØAD4 card.
4. If the alternate form is used, all elements in the range EID1 through EID2 must be present.

5. The "work equivalent" load vector is computed for each element using the relation

$$\vec{F} = P \int_{-1}^{1} \int_{-1}^{1} [\bar{N}]^T \vec{v}_n \det [J] \, d\xi \, d\eta$$

6. All elements referenced must exist.

Input Data Card SHLNORM Shell Normal

Description: Defines the direction of a normal to the shell of the structural model.

Format and Example:

1	2	3	4	5	6	7	8	9	10
SHLNORM	ID	CP	X1	X2	X3				
SHLNORM	2	3	1.0	2.0	3.0				

Field	Contents
ID	Grid point identification number (0 < Integer < 999999) at which this normal is located.
CP	Identification number of coordinate system in which the shell normal is defined (Integer ≥ 0 or blank).
X1,X2,X3	Components of the shell normal in coordinate system CP (Real).

Remarks:

1. All grid point identification numbers must be unique with respect to all other structural, scalar, and fluid points.
2. The meaning of X1, X2 and X3 depend on the type of coordinate system, CP, as follows: (see CØRD ___ card descriptions).

Type	X1	X2	X3
Rectangular	X	Y	Z
Cylindrical	R	Θ(degrees)	Z
Spherical	R	Θ(degrees)	Φ(degrees)

REFERENCES

1. Ahmad, S., Irons, B. M. and Zienkiewicz, O. C., "Analysis of Thick and Thin Shell Structures by Curved Finite Elements", Int. J. Num. Meth. Engr., Vol. 2, pp. 419-451, 1970.

2. Cowper, G. R., Lindberg, G. M. and Olson, M. D., "A Shallow Shell Finite Element of Triangular Shape", Int. J. Solids Structures, Vol. 6, 1970, pp. 1133-1156.

3. Dupuis, G. and Goel, J. J., "A Curved Finite Element for Thin Elastic Shells", Brown University Engineering Report N00014-Q007/4, December, 1969.

4. Zienkiewicz, O. C., Taylor, R. L. and Too, J. M., "Reduced Integration Technique in General Analysis of Plates and Shells", Int. J. Num. Meth. Engr., Vol. 3, pp. 275-290, 1971.

5. Pawsey, S. F. and Clough, R. W., "Improved Numerical Integration of Thick Shell Finite Elements", Int. J. Num. Meth. Engr., Vol. 3, pp. 575-586, 1971.

6. Barsoum, R. S., "A Degenerate Solid Element for Linear Fracture Analysis of Plate Bending and General Shells", Int. J. Num. Meth. Engr., Vol. 10, pp. 551-564, 1976.

7. Wergeland, J. H., User's Manual for Program SCQS31 (part of DnV's SESAM program) 31.10.73/01.

8. Hinton, E., Razzaque, A., Zienkiewicz, O. C. and Davies, J. D., "A Simple Finite Element Solution for Plates of Homogeneous, Sandwich and Cellular Construction", Proc. Instn. Civ. Engrs. (London), Part 2, 59, pp. 43-65, March 1975.

9. Irons, B. M. and Hellen, T. K., Short Communication on "On Reduced Integration in Solid Isoparametric Elements When Used in Shells with Membrane Modes", Int. J. Num. Meth. Engr., Vol. 10, pp. 1179-1182, 1975-76.

10. Timoshenko, S. P. and Woinowsky-Krieger, S., Theory of Plates and Shells, 2nd Edition, McGraw-Hill, 1959.

11. Cantin, G. and Clough, R. W., "A Curved, Cylindrical-Shell Finite Element", AIAA Journal, Vol. 6, No. 6, June 1968, pp. 1057-1062.

12. Scordelis, A. C. and Lo, K. S., "Computer Analysis of Cylindrical Shells", Journal of the American Concrete Institute, 61, 1964, pp. 539-561.

13. Gibson, J. E., The Design of Cylindrical Shell Roofs, 2nd Edition, E.&F.N. Spon, 1961.

14. Anon., MARC-CDC User Information Manual, Vol. I-III, Revision J, CDC Publications and Graphics Division, 1977.

15. Nicolos, V. T. and Citipitioglue, E., "SDRC SUPERB, A General Isoparametric Finite Element Program", Paper presented at the Second National Symposium on Computerized Analysis and Design, George Washington University, March 29-31, 1976.

16. Zienkiewicz, O. C., The Finite Element Method in Engineering Science, McGraw-Hill, 1971, p. 353-354.

17. Leick, R. D. and Potvin, A. B., "Automated Mesh Generation for Tubular Joint Stress Analysis," Second National Symposium on Computerized Structural Analysis and Design, George Washington University, March 29-31, 1976.

18. Katnik, R., "A Note on Moment Balance in the Isoparametric Shell Element," Int. J. Num. Meth. Engr., Vol. 11, No. 1, pp. 199-200, 1977.

TABLE 1. DISPLACEMENT CONVERGENCE FOR CYLINDRICAL SHELL ROOF

GRID	V_A	W_B	U_B	W_C	
1 x 1	-0.226	-9.609	-5.413	1.801	cm
	-0.089	-3.783	-2.131	0.709	in.
2 x 2	-0.368	-8.966	-4.752	1.313	cm
	-0.145	-3.530	-1.871	0.517	in.
3 x 3	-0.381	-9.241	-4.879	1.346	cm
	-0.150	-3.638	-1.921	0.530	in.
4 x 4	-0.381	-9.208	-4.854	1.379	cm
	-0.150	-3.625	-1.911	0.543	in.
EXACT	-0.384	-9.406	-4.986	1.334	cm
	-0.150	-3.703	-1.963	0.525	in.

FIGURE 1. ELEMENT GEOMETRY AND LOCAL COORDINATE SYSTEMS

FIGURE 2. CONVERGENCE STUDY FOR SIMPLY-SUPPORTED FLAT PLATE

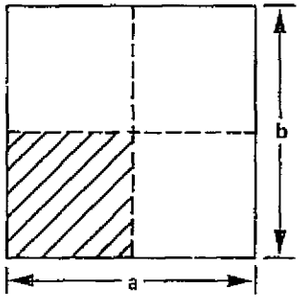

$E = 69.4\ KN/mm^2\ (1.0 \times 10^7\ psi)$

$\nu = 0.3$

a = b = 254 mm (10 in.)

t = 2.54 mm (0.1 in.)

$P = 178.4\ N\ (40\ lb.),\ 6.94\ KN/m^2\ (1.0\ psi)$

GRID	VERTICAL DEFLECTION AT CENTER			
	CENTRAL LOAD		UNIFORM PRESSURE	
	mm	in.	mm	in.
1 x 1	-1.286	-5.062×10^{-2}	-1.214	-4.778×10^{-2}
2 x 2	-1.284	-5.054×10^{-2}	-1.142	-4.498×10^{-2}
3 x 3	-1.294	-5.095×10^{-2}	-1.143	-4.50×10^{-2}
4 x 4	-1.295	-5.098×10^{-2}	-1.139	-4.483×10^{-2}
TIMOSHENKO	-1.287	-5.068×10^{-2}	-1.128	-4.44×10^{-2}

FIGURE 3. CONVERGENCE STUDY FOR PINCHED CYLINDER PROBLEM

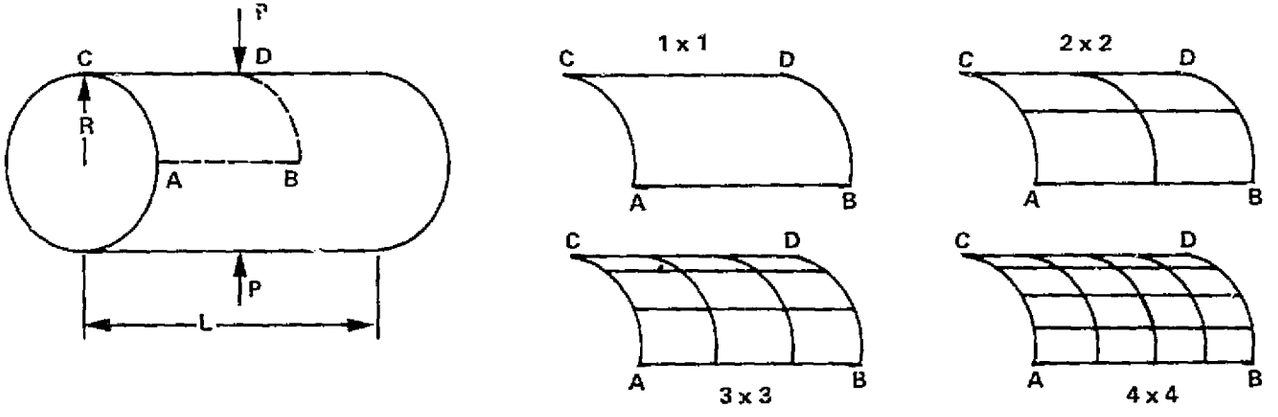

E = 72.9 KN/mm^2 (10.5 x 10^6 psi)

ν = 0.3125

R = 125.8 mm (4.953 in.)

L = 262.9 mm (10.35 in.)

t = 2.39 mm (0.094 in.)

P = 445.9 N (100 lb.)

GRID	DOF (TOTAL)	RADIAL DISPLACEMENT AT POINT D	
		mm	in.
1 x 1	40	-2.517	-0.991×10^{-1}
2 x 2	105	-2.753	-1.084×10^{-1}
3 x 3	200	-2.863	-1.127×10^{-1}
4 x 4	325	-2.893	-1.139×10^{-1}
TIMOSHENKO		-2.761	-1.087×10^{-1}

FIGURE 4. MESH CONFIGURATIONS FOR CYLINDRICAL SHELL ROOF

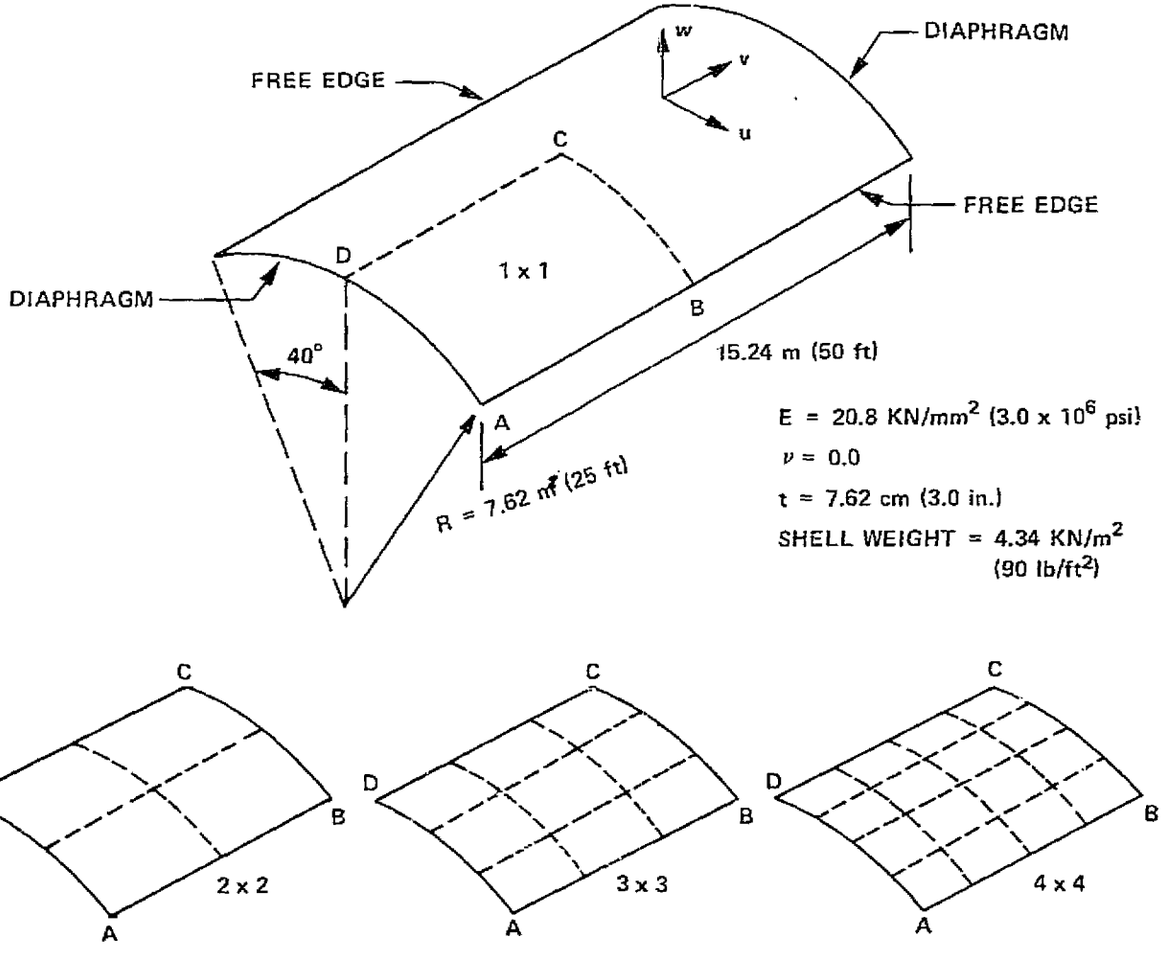

FIGURE 5. ELEMENT CONVERGENCE COMPARISON FOR CYLINDRICAL ROOF PROBLEM

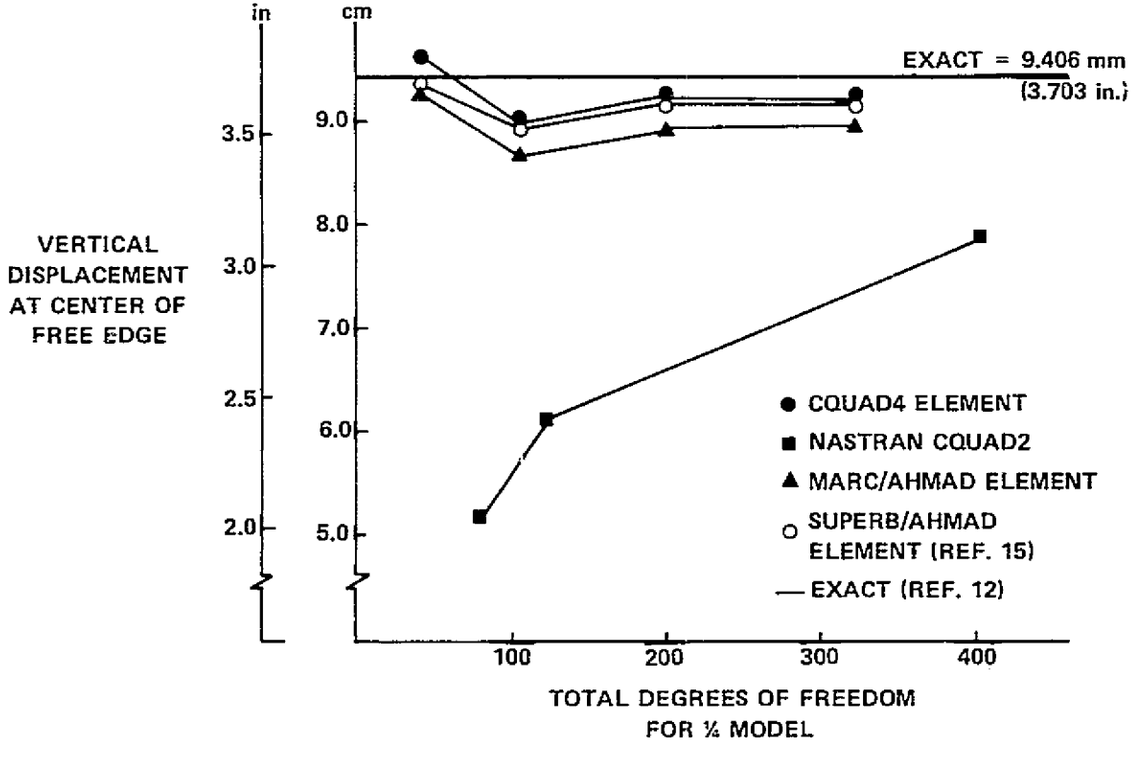

FIGURE 6. FREE VIBRATION OF A CANTILEVER PLATE

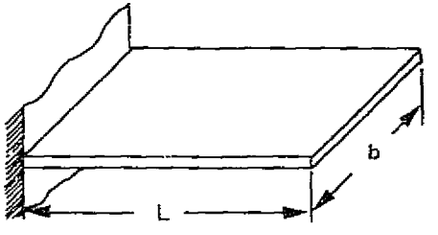

E = 208.3 KN/mm^2 (3.0×10^7 psi)

ν = 0.3

e = 7.85 t/m^3 (0.283 lb/in^3)

L = 50.8 mm (2.0 in.)

b = 25.4 mm (1.0 in.)

t = 2.54 mm (0.1 in.)

MODE	$\omega/\sqrt{D/\rho t L^4}$				
	EXPERIMENTAL (PLUNKETT)	NON-CONFORMING TRIANGLE ZIEN KIEWICZ		CQUAD4 ELEMENT	
		2 x 1	4 x 2	2 x 1	4 x 2
1	3.50	3.39	3.44	3.45	3.43
2	14.50	15.30	14.76	14.64	14.43
3	21.70	21.16	21.60	22.63	21.30
4	48.10	49.47	48.28	49.79	46.82
5	60.50	67.46	60.56		60.55
6	92.30		88.84		90.76
7	92.80		92.24		97.17
8	118.70		117.72		123.05
9	125.10		118.96		130.23
10	154.00				

FIGURE 7. DEGENERACY RESULTING FROM NON-RECTANGULARITY

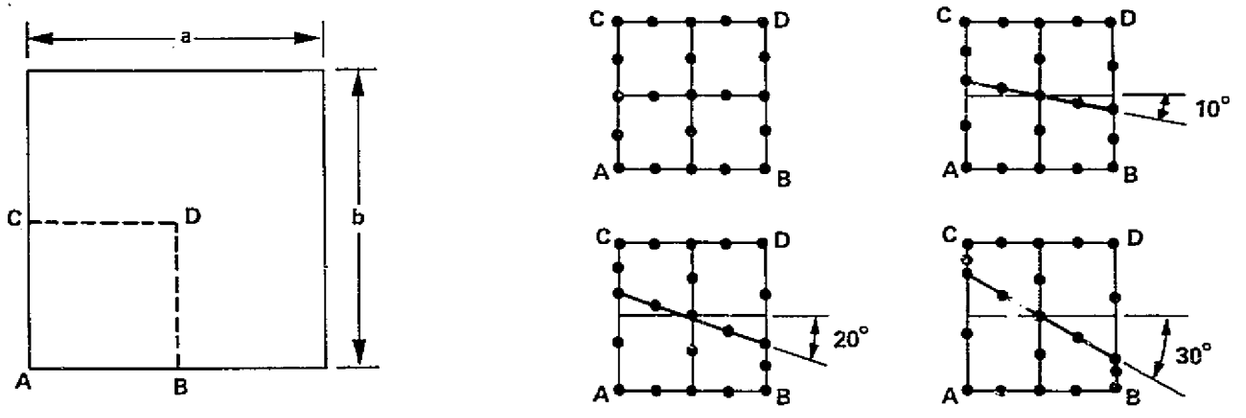

E = 69.4 KN/mm^2 (1.0 x 10^7 psi)

ν = 0.3

a = b = 254 mm (10 in.)

t = 2.54 mm (0.1 in.)

P = 6.94 KN/m^2 (1.0 psi)

GRID	VERTICAL DISPLACEMENT AT POINT D	
	mm	in.
RECTANGULAR	-1.143	-4.498×10^{-2}
10° OFFSET	-1.145	-4.506×10^{-2}
20° OFFSET	-1.118	-4.403×10^{-2}
30° OFFSET	-1.059	-4.169×10^{-2}
TIMOSHENKO	-1.128	-4.44×10^{-2}

FIGURE 8. DEGENERACY DUE TO THINNESS RATIO

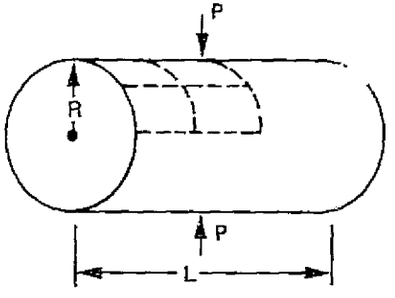

$E = 69.4\ KN/mm^2\ (1.0 \times 10^7\ psi)$

$\nu = 0.3$

R = 25.4 cm (10.0 in.)

L = 50.8 cm (20.0 in.)

P = 445.9 N (100 lb)

$$q_{max} = -\frac{1}{2}(0.149)\frac{P R^3}{2D (L/2)}$$

$$q_{max}\, D = -1.0716 \times 10^6\ N\ mm^2$$

t/R	D (N mm)	q_{max} (mm)	$(q_{max})(D)$
0.1	1.041×10^8	-1.185×10^{-2}	-1.234×10^6
0.01	1.041×10^5	-1.035×10^1	-1.078×10^6
0.001	1.041×10^2	-1.024×10^4	-1.066×10^6
0.0001	1.041×10^{-1}	-1.024×10^7	-1.066×10^6

FIGURE 9. DEGENERACY DUE TO MISALIGNMENT WITH DIRECTIONS OF PRINCIPAL CURVATURE

*NOTE USE OF DEVELOPED SURFACE COORDINATES

FIGURE 10. SUBSTRUCTURE MESHES FOR TYPICAL T-JOINT

NOTE USE OF DEVELOPED SURFACE COORDINATES

FIGURE 11. SUBSTRUCTURE MESHES FOR TYPICAL K-JOINT

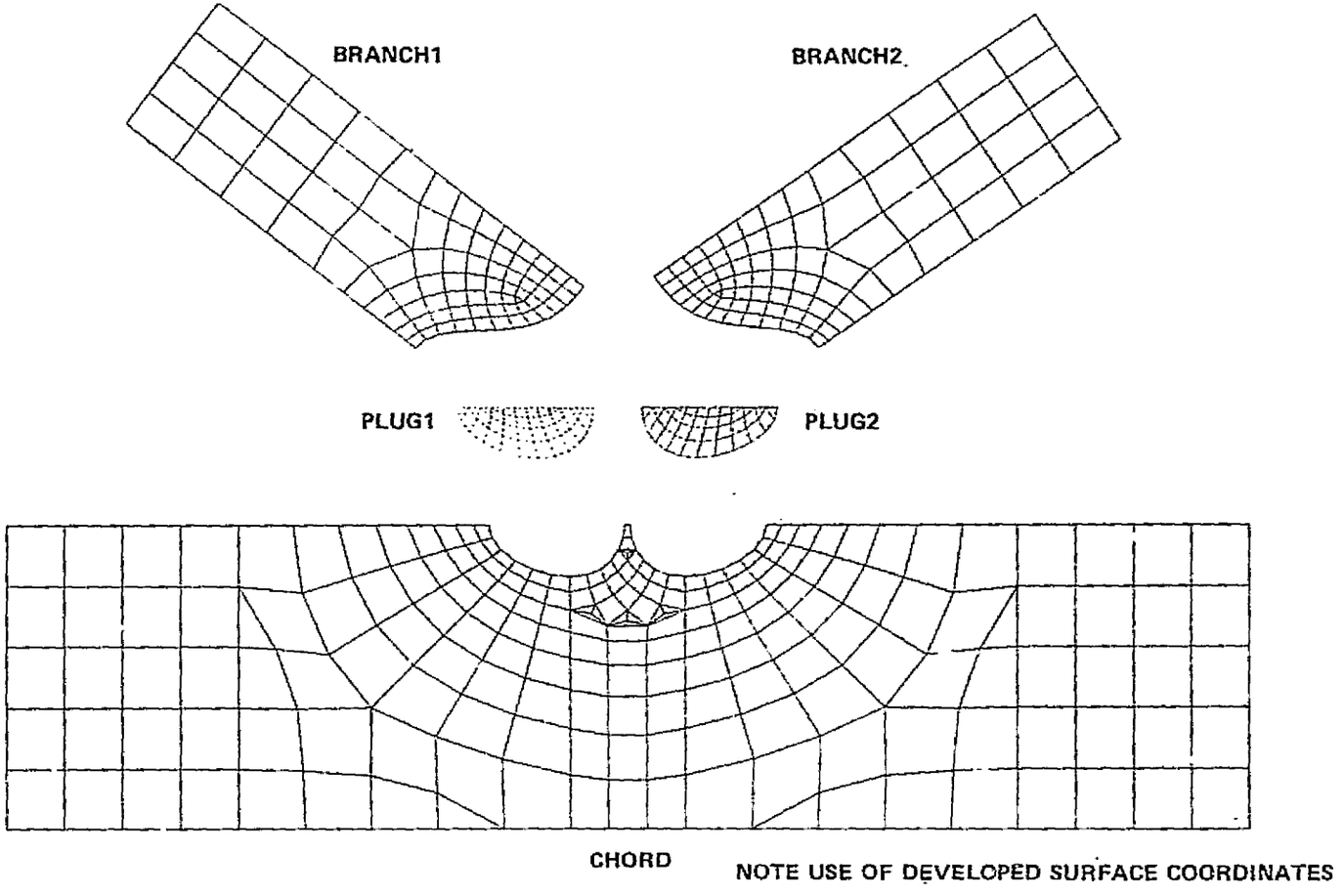

FIGURE 12. TYPICAL CONCRETE GRAVITY STRUCTURE